minerals

MDPI

Article

The Petrogenesis of the Gaohushan A-Type Granite from the Northeastern Jiangxi Province and Its Metallogenic Implication

Zhanqing Liu [1], Fengzhi Cui [1,2,*] and Saisai Li [1]

[1] Guangxi Key Laboratory of Hidden Metallic Ore Deposits Exploration, College of Earth Science, Guilin University of Technology, Guilin 541004, China; lzqgygcx2008@163.com (Z.L.)
[2] Earthquake Agency of Inner Mongolia Autonomous Region, Hohhot 010051, China
* Correspondence: cuifengzhi@nmgdzj.gov.cn

Abstract: The Taqian–Zhuxi–Fuchun metallogenic belt in northeastern Jiangxi Province contains significant ore deposits that are closely associated with the Gaohushan granites. The Gaohushan granites predominantly consist of two-mica granites and have been dated using zircon U-Pb isotopic dating to be 129.4 ± 1.9 Ma (MSWD = 3.8). These granites have high SiO_2, ranging from 73.79% to 76.04% and low CaO and MgO contents (ranging from 0.24% to 0.59% and from 0.03% to 0.1%, respectively). The Gaohushan granites also exhibit high FeO^T/MgO ratios from 9.00 to 27.55 with an average of 17.55. The total alkali contents (Na_2O + K_2O) range from 7.08% to 8.43%, and the K_2O/Na_2O ratios range from 1.07 to 2.00 with an average of 1.47. These rocks are peraluminous series with A/CNK ratios (or ASI index) ranging from 1.19 to 1.47 and an average of 1.30. The Gaohushan granites have low rare earth element (REE) contents (∑REE = 2.33~23.50) with strongly negative Eu anomalies (δEu from 0.02 to 0.32) and a distinctive differentiation between heavy rare earth elements (HREEs) and light rare earth elements (LREEs) (LREE/HREE = 1.99~7.79). The normalized distribution pattern of REE in Gaohushan granite exhibits a right-dipping feature classified A-type; these rocks range from 1.06 to 2.71. The spider diagram shows that these rocks are characterized by depletion of Ba, Th, La, Sr, Nd, and Ti and enrichment of Rb, U, Ta, Nb, and P. The Gaohushan granites are classified as A-type granite and were emplaced during an anorogenic extensional event that occurred in the late Yanshannian period, driven by mantle-derived magma underplating. It is these granites or their analogues that have the potential for hosting tungsten, tin, niobium, and tantalum deposits, making them a promising target for mineral exploration.

Keywords: northeastern Jiangxi province; Gaohushan granitoids; A-type granite; zircon U-Pb dating; prospecting potential

Citation: Liu, Z.; Cui, F.; Li, S. The Petrogenesis of the Gaohushan A-Type Granite from the Northeastern Jiangxi Province and Its Metallogenic Implication. *Minerals* **2023**, *13*, 588. https://doi.org/10.3390/min13050588

Academic Editor: Aleksei V. Travin

Received: 15 March 2023
Revised: 12 April 2023
Accepted: 20 April 2023
Published: 23 April 2023

1. Introduction

The Qin–Hang belt in South China is the collision suture zone between the Yangtze block and the Cathaysia block during the Late Proterozoic period [1,2]. Although the southwest section of the belt remains controversial [3–5], the location and characteristics of the Jiangshan–Shaoxing fault zone in the northeast section have been widely verified, particularly the fault zone in northeastern Jiangxi province (Figure 1a) [6–8]. During the middle to late Jurassic period, this belt experienced intense magmatic activity and the formation of several polymetallic deposits including copper, gold, tungsten, tin, lead, and zinc. These deposits have given rise to a large intra-plate polymetallic metallogenic belt in the Qin–Hang region [9–12]. In recent years, several world-class deposits have been discovered in this belt, including the Dexing porphyry Cu deposit and the Zhuxi skarn Cu-W deposit [13,14]. These polymetallic deposits are closely associated with the intermediate-acid magmatism and tectonic activity in the Qin–Hang belt. Therefore, the study of granites in this region can provide valuable information for mineral prospecting in the area.

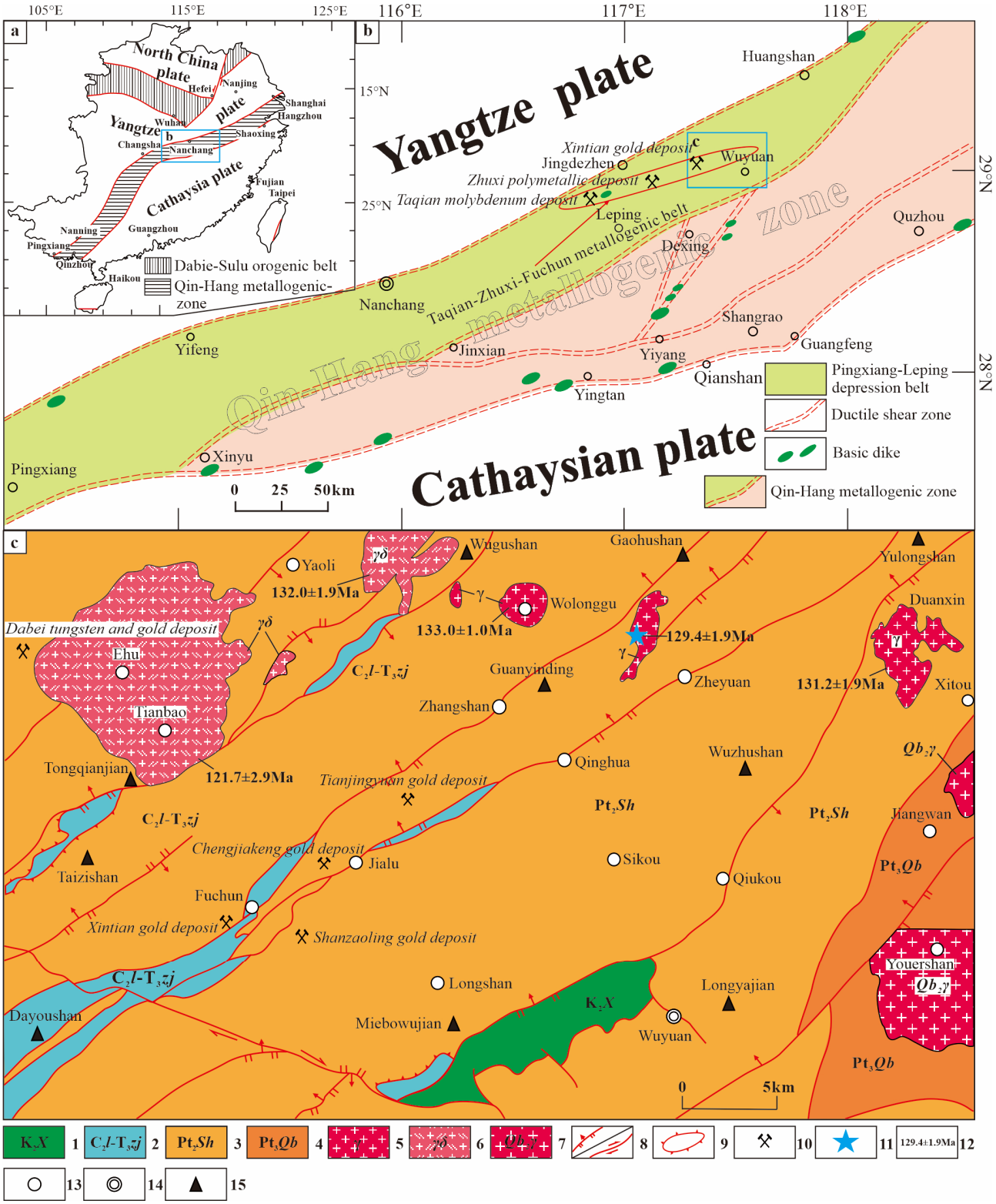

Figure 1. (**a**) Geological map of Gaohushan area in the northeastern Jiangxi province. (**b**) Qin-Hang metallogenic zone. (**c**) Geological map of Gaohushan area in the northeastern Jiangxi province.1: Cretaceous; 2: Late Carboniferous–Triassic; 3: Neoproterozoic Shuangqiaoshan Group; 4: Neoproterozoic Qingbaikou strata; 5: Yanshanian granite; 6: Yanshanian granodiorite; 7: Jinningian granite; 8: reverse fault and strike-slip fault; 9: tectonic window; 10: gold deposit; 11: sampling location; 12: granitoid pluton age; 13: county; 14: city; 15: mountain.

The Gaohushan pluton is situated at the northeastern margin of the Taqian–Zhuxi–Fuchun metallogenic belt. The Taqian–Zhuxi–Fuchun metallogenic belt is located between Taqian in Leping city, northeast of Jiangxi Province, and Fuchun county in Wuyuan city. It is located in the eastern part of the Pingxiang–Leping depression belt and is a component of the depression belt, with a total length of approximately 121 km. This belt is known for its intense magmatism, which includes mafic-ultramafic and intermediate-acid magmatic rocks, with intermediate-acid magmatic rocks being dominant. The major periods of magmatic activity include the Jinning period in the early Mesoproterozoic, the Hercynian period in the late Paleozoic, and the Yanshanian period in the early to late Mesozoic, with the Yanshanian period being the most prominent. The latest Yanshannian period can be divided into three stages: early Yanshanian (ca. 160~170 Ma), middle Yanshanian (ca. 140~150 Ma), and late Yanshanian (ca. 120~130 Ma) [15,16]. Adjacent magmatic rocks near the Gaohushan pluton include Duanxin pluton (two-mica granite, 131.2 ± 1.9 Ma) [17], Wolonggu pluton (Mesozoic granite, 133.0 ± 1 Ma) [18], Yaoli pluton (biotite Mesozoic granite, 132.0 ± 1.9 Ma) [19], Jincun pluton, Taoling pluton and Ehu pluton (Mesozoic granite, 121.7 ± 2.9 Ma) [20] with distribution in E-W direction (Figure 1b). There is still controversy surrounding the petrogenesis of these plutons, particularly regarding the relationship between tectono-magmatism and the metallogenic process in the belt. Therefore, we are focusing on the Gaohushan pluton and conducting precise geochemical and zircon U-Pb dating analyses to elucidate its petrogenesis and its relationship with mineral deposits.

2. Regional Geological Setting

The Gaohushan region is in the northeastern part of Jiangxi Province, at the southeastern margin of the Yangtze plate. It falls within the Jiangxi section of the Qin–Hang belt, which is located between the Yangtze and Cathaysian blocks. The region is part of the Taqian–Zhuxi–Fuchun secondary metallogenic belt, which is known for its Cu–Au–Pb–Zn–Nb–Ta mineralization in the Jiangnan orogenic belt. The Gaohushan region is in the northwestern stratigraphic zone of the northeastern Jiangxi deep fault belt, at the eastern end of the Pingxiang–Leping depression belt within the Jiangnan ancient island arc belt (Figure 1c). It is situated between the Jiuling and Wannian uplifting zones, forming a tectonic framework of "one depression sandwiched between two uplifts" [1]. The strata in this region are characterized by their unique geological features and have attracted significant research attention [21]. The northeastern Jiangxi Province is dominated by a low-grade greenschist metamorphic facies flysch formation consisting of argillaceous and sandy fine-grained clastic rocks with minor volcanics. This flysch formation, together with other contemporaneous strata, forms a major part of the Jiangnan orogenic belt and provides important constraints on the tectonic evolution of this region, which has had significant implications for the entire South China region since the Neoproterozoic [22].

The NE-trending deep fault zones, such as the Yiyang–Dexing and Yifeng–Jingdehen–Qimen fault zones in northeastern Jiangxi province, exerted significant control on magma intrusion and gold mineralization in the ductile shear belt northwest of these intrusions [23]. Shallow metamorphic sedimentary rocks of the Neo–Proterozoic Shuangqiaoshan Group are widely distributed in the region [24]. The Carboniferous to Triassic marine carbonate rocks, coal-bearing formations, and clastic rocks of marine-terrigenous facies, as well as the Jurassic and Cretaceous red sedimentary basins, are zonally distributed in a northeast direction. The region also contains a series of large-scale granitic rocks that intruded into the Shuangqiaoshan Group and outcropped in the area, such as the Jinningian Shi'ershan A-type granite and the Early Cretaceous Ehu S-type granite [20,25]. These smaller granitic plutons in this region include Gaohushan, Wolonggu, Yaoli, Jincun, Taoling and other intrusions, as well as a small amount of diorite porphyrite and quartz diorite dikes. The Gaohushan granitic pluton is distributed along the direction of NNE along the fault zone. The Gaohushan pluton is in short strip shape with an outcrop of ~5 km in length and 2 km in width (Figure 1b).

3. Petrography

The Gaohushan pluton is mainly composed of two-mica granite, which is like the adjacent Wolonggu and Youli plutons. The Gaohushan pluton intruded the metamorphic basement of the Neoproterozoic Shuangqiaoshan Group and was cut by a NE-trending thrust fault. The two-mica granite of Gaohushan exhibits a medium-fine grained granitic texture. The Gaohushan two-mica granite mainly consists of quartz (~40%), K-feldspar (~25%), plagioclase (~20%), muscovite (~5%) and biotite (5%), with minor accessory phases, e.g., magnetite, zircon, apatite (<5%). The K-feldspar shows Carlsbad twin crystal. The plagioclase shows polycrystalline twin crystal. Both the K-feldspar and plagioclase show weak sericite alteration, while the biotite shows weak chloritized alteration (Figure 2).

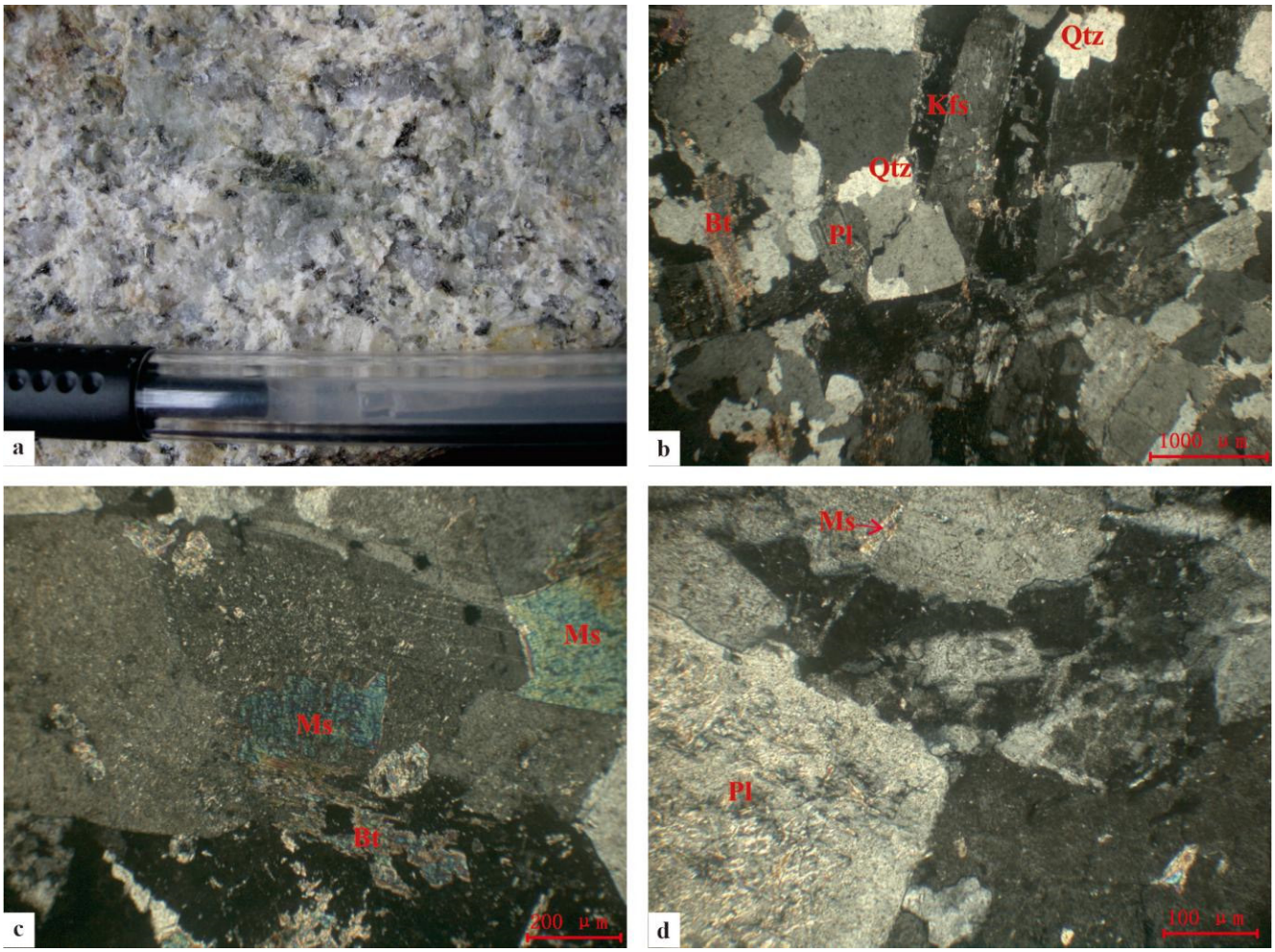

Figure 2. Hand specimens and microscopic photos of the Gaohushan granite in the northeastern Jiangxi province. (**a**) Rock hand specimen; (**b**) mineral assemblage under orthogonal polarizer; (**c**) muscovite and biotite; (**d**) Qtz: quartz; Bt: biotite; Ms: muscovite; Kfs: feldspar; Pl: plagioclase.

4. Analytical Methods

4.1. Zircon U-Pb Dating

One sample of the Gaohushan granite (Sample No. GHSH) was collected and used for zircon U-Pb dating by laser ablation inductively coupled plasma mass spectrometry (LA-ICP-MS). The geographical coordinates of this sample are 29°29′59″ N, 117°51′57″ E (Figure 1). Firstly, the sample was ground to ~60 mesh, then zircons were selected by conventional manual panning and magnetic separation methods. These zircons with better crystal shape were picked under a binocular microscope. These zircons were fixed in a target with colorless epoxy resin, then ground and polished. The reflected light and

cathodoluminescence (CL) photomicrographs of these zircons were carried out at the Beijing SHRIMP Center. Zircon U-Pb dating was analyzed by the LA-ICP-MS at the State Key Laboratory of Continental Dynamics, Northwest University. Zircon age calculation and diagram drawing were performed using the ISOPLOT program [26].

4.2. Whole Rock Major and Trace Elements

The sample fragmentation was performed at the Geological and Mineral Investigation Research Laboratory in Langfang City, Hebei Province. The samples were ground to 200 mesh. The major and trace element analyses of the whole rocks were conducted at the Key Laboratory of Western Mineral Resources and Geological Engineering of the Ministry of Education, Chang'an University.

For major element analysis, approximately 0.9 g of devolatilized or ignited sample was mixed with lithium borate flux (~9.0 g, 50% $Li_2B_4O_7$-$LiBO_2$) and fused in an auto fluxer at a temperature of approximately 1100 °C. The resulting molten glass disk was then cooled and analyzed using the Japanese LAB CENTER XRF-1800 X-ray fluorescence spectrometer. The analytical precisions for the major elements are as follows: SiO_2 (0.8%), Al_2O_3 (0.5%), Fe_2O_3 (0.4%), MgO (0.4%), CaO (0.6%), Na_2O (0.3%), K_2O (0.4%), MnO (0.7%), TiO_2 (0.9%), and P_2O_5 (0.8%).

The trace element concentrations, including rare earth elements (REE), were determined using an American X-7 inductively coupled plasma mass spectrometer. Prior to analysis, the samples were placed in Teflon screw-cap bombs and digested in a mixture of 1.0 mL high-purity hydrofluoric acid (HF) and 1.5 mL high-purity nitric acid (HNO_3) using closed beaker digestion for two days. The resulting dissolved samples were then diluted to 50 mL with 2% nitric acid (HNO_3) before analysis. The analytical precision of the method was generally better than 5%.

5. Results

5.1. Zircon U-Pb Geochronology

Most zircons in (Sample No. GHSH) exhibit a transparent or light yellow, prismatic, and euhedral morphology. These zircons range from 50 to 200 μm in diameter. The cathodoluminescence (CL) photos show that these zircons have a typical magma oscillatory zoning, indicating their magmatic origin (Figure 3). Some zircons (e.g., zircon grain of 02) have relict core. The zircon U-Pb dating results are listed in Tables S1 and S2. Twenty-five zircons have high Th and U contents, ranging from 38 to 381 ppm and from 88 to 3088 ppm, respectively. Most zircons have higher Th/U ratios than 0.1 (except for zircon grains of 10, 14, and 20), also implying a magmatic origin. According to the chondrite normalized REE distribution patterns of zircons (Figure 4), they show strong fractionation between LREE and HREE, with positive Ce anomalies and negative Eu anomalies, further indicating a magmatic origin [27,28]. In the concordia diagram, all the zircons plotted on or near the concordia line and the twenty-four zircons (except for the zircon grain of 02) yield a weighted mean $^{206}Pb/^{238}U$ age of 129.4 ± 1.9 Ma (n = 24, MSWD = 3.8, 2σ) (Figure 4a). The dating results reveal that the Gaohushan granite was formed during the Early Cretaceous period, indicating its crystallization time.

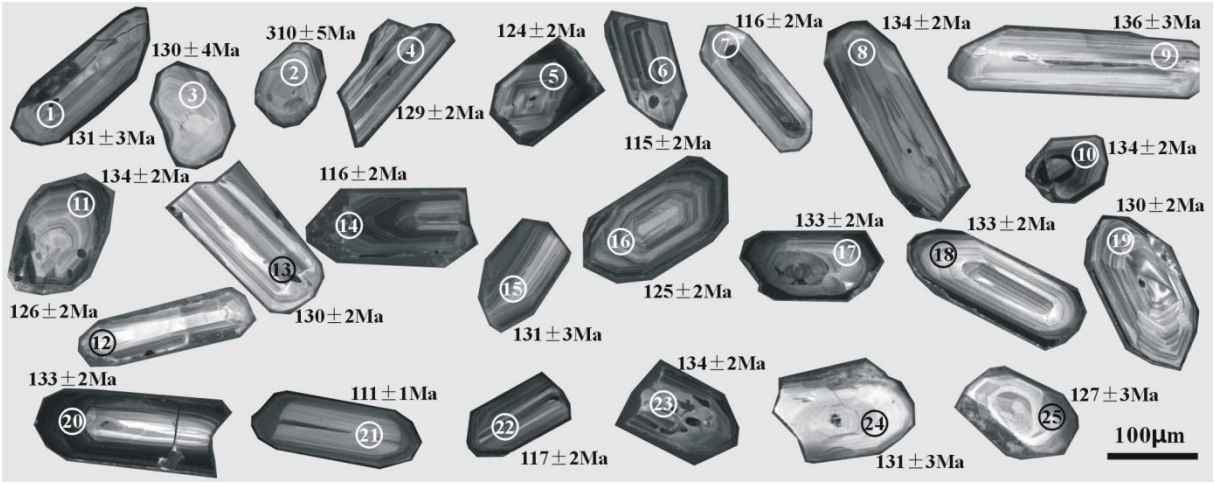

Figure 3. Cathodoluminescence images, analyzed location, and ages of analyzed zircons from the Gaohushan granite.

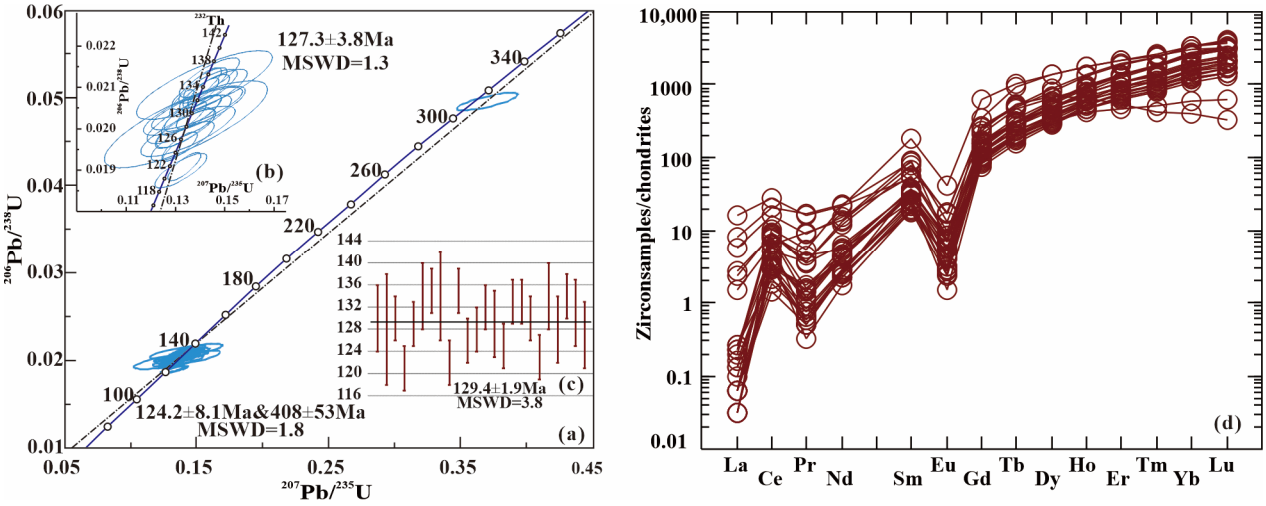

Figure 4. (**a**,**b**) U-Pb concordia diagrams; (**c**) weighted mean age; (**d**) chondrite-normalized REE distribution patterns of zircons from the Gaohushan granite, northeastern Jiangxi province (chondrite data for normalization are from [29]).

5.2. Whole Rock Major and Trace Elements Compositions

5.2.1. Major Elements

The major and trace element compositions of Gaohushan granites can be found in Table S3. The granites are characterized by high SiO_2 and Al_2O_3 contents, which range from 73.79% to 76.04% and from 13.60% to 14.52%, respectively. The total alkali contents ($Na_2O + K_2O$) range from 7.08% to 8.43%, while K_2O/Na_2O ratios range from 1.07 to 2.00. In the TAS diagram, all samples of two-mica granite are located within the granite area (Figure 5). In the QAP diagram, all samples of two-mica granite are located within the monzogranite area (Figure 6). The Gaohushan granites have high FeO^T/MgO ratios ranging from 9.00 to 27.55, with an average value of 17.55, but low CaO and MgO contents (ranging from 0.24% to 0.59% and from 0.03% to 0.1%, respectively). The $Mg^{\#}$ values of these two-mica granites range from 6.19 to 14.92, with an average value of 10.17. The A/CNK ratios (or ASI index) of these granites range from 1.19 to 1.47, with an average value of 1.30. In the A/NK vs. A/CNK diagram, all the granites are plotted in the peraluminous area, indicating high levels of aluminum saturation (Figure 7a). According to the CIPW standard mineral calculation, it can be observed that all the samples contain corundum (C)

with an average content of 3.97%, ranging from 2.91% to 5.24%, which indicates that these granites are strongly peraluminous. Additionally, all the granites belong to the high-K calc-alkaline series (Figure 7b). The Ritterman indices (σ43), differentiation indices (DI), and consolidation indices (SI) of these granites range from 1.58 to 2.27, 91.09 to 95.12, and 0.34 to 1.14, respectively.

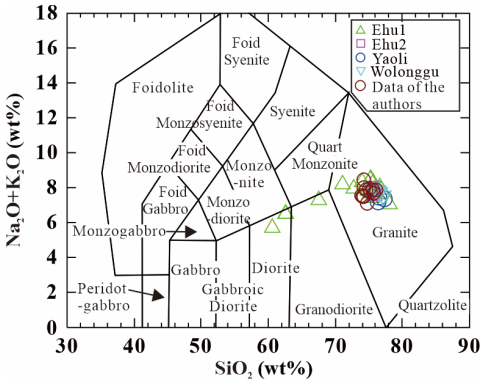

Figure 5. TAS diagram of Gaohushan granites and adjacent intrusions (modified after [30]). Data sources of Gaohushan adjacent intrusions: Ehu1 [31]; Ehu2 [20]; Yaoli [19]; Wolonggu [32].

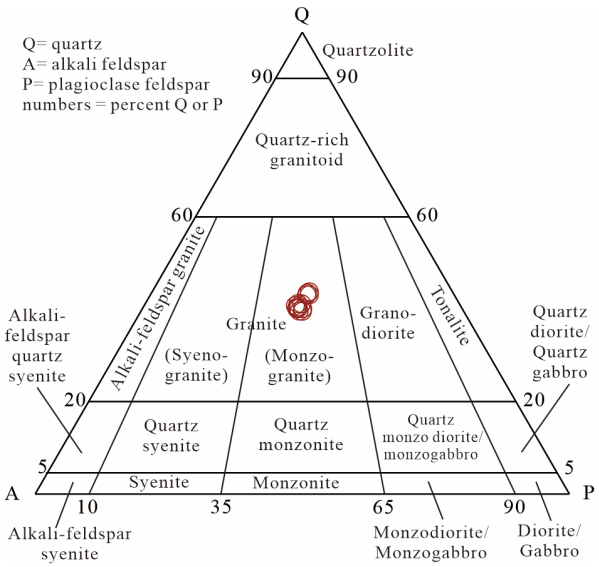

Figure 6. QAP diagram of Gaohushan granites (modified after [33]). (data sources and legends shown in Figure 5).

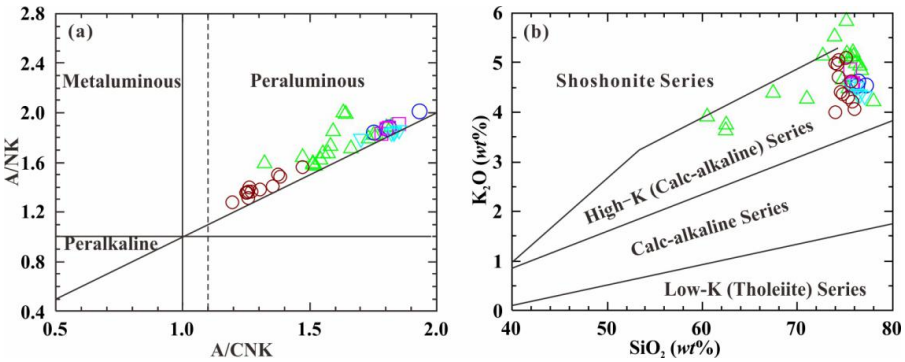

Figure 7. (**a**) A/NK vs. A/CNK (modified after [34]); (**b**) K_2O vs. SiO_2 diagrams for Gaohushan granites and adjacent intrusions (modified after [34]). (data sources and legends shown in Figure 5).

5.2.2. Trace and Rare Earth Elements

The Gaohushan granites exhibit low contents of rare earth elements (REEs) ranging from 2.33 to 23.50 ppm, with an average value of 7.48 ppm. There is a slight differentiation between light rare earth elements (LREEs) and heavy rare earth elements (HREEs), with LREE/HREE and $(La/Yb)_N$ ratios ranging from 1.99 to 7.79 and 1.45 to 16.65, respectively. The granites also show significant negative Eu anomalies with δEu ranging from 0.02 to 0.32. Additionally, the normalized distribution pattern of REE in chondritic meteorites displays a right-dipping feature (Figure 8a). The Gaohushan granites exhibit an average $10^4 \times Ga/Al$ ratio of 2.11, with a range from 1.06 to 2.71. These granites also display low contents of Zr + Y + Nb + Ce, ranging from 23.61 to 84.22 ppm. Primitive mantle normalized trace element spider diagrams indicate that these rocks are depleted in Ba, Th, La, Sr, Nd, and Ti, but enriched in Rb, U, Ta, Nb, and P (Figure 8b).

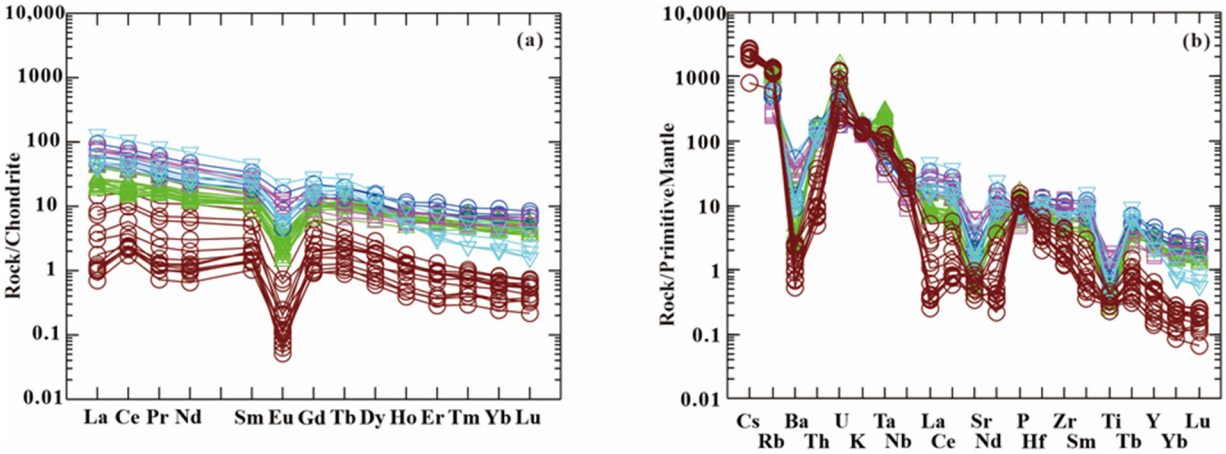

Figure 8. (**a**) Chondrite normalized REE distribution patterns; (**b**) primitive mantle normalized spider diagram of trace elements of Gaohushan granites and adjacent intrusions (chondrite and primitive mantle data for normalization are from [29]). (data sources and legends shown in Figure 5).

6. Discussion

6.1. Petrogenesis

The Gaohushan granites are characterized by high SiO_2 contents and a strong peraluminous nature. They also exhibit higher FeO^T/MgO ratios, ranging from 9.00 to 27.55, compared to the average of 2.27 for I-type granite [35]. The REE distribution patterns of the Gaohushan granites exhibit characteristics like those of peraluminous A-type granite. The Gaohushan granite has a relatively low content of rare earth elements (REE), with a range of ∑REE between 2.33 to 23.50 ppm, similar to other A-type granites [36]. Compared to the average REE content of A-type granite in the Zhenzhushan area (~17.01 ppm), the Late Yanshanian fine-grained alkali feldspar granite in Hunan Xitian area (~28.78 ppm), and the A-type granite in Daxinganling Woduhe area (~46.52 ppm) [36,37], the REE content of Gaohushan granite is relatively lower.

For high-silicon granites (SiO_2 > 74%), the FeO^T/MgO vs. SiO_2 diagram can effectively differentiate A-type granites from I-type and S-type granites. The Gaohushan granite samples are plotted in the A-type area [38] (Figure 9a), indicating their classification as A-type magmatism. Similarly, the Na_2O vs. K_2O diagram also shows that the Gaohushan granites belong to an A-type magmatism (Figure 9b).

The Gaohushan granites are plotted in the peraluminous area in the A/NK vs. A/CNK diagram (Figure 9a) and are showing a strongly peraluminous characteristic. Rb, Sr, and Ba in granite are mainly enriched in feldspar and biotite. The ratios of Rb/Ba and Rb/Sr can reflect the source area for the strong peraluminous granite. The Rb/Ba ratios of the Gaohushan granites are from 41 to 196, and higher than granites in Ehu, Yaoli, and Wolonggu areas, indicating an increasing proportion of clay in the magmatic source [39]

(Figure 9c). The CaO/Na_2O ratio of granite with the argillaceous source is generally less than 0.3 [40], and CaO/Na_2O ratios of the Gaohushan granite are from 0.08 to 0.19 (with an average value of 0.13), indicating that the source of Gaohushan granite is mainly argillaceous (Figure 9d).

Highly differentiated acid magma can give rise to strong peraluminous A-type granites, with the Zr/Hf ratios serving as a useful indicator of the degree of magma crystallization differentiation [41]. Breiter [41] noted that the granitoids do not contain any other real host of Zr and Hf besides zircon. Therefore, average Zr/Hf values in zircon should equal average Zr/Hf values in the whole rock. Based on Zr/Hf ratios, granite can be classified into three types: ordinary granite (Zr/Hf > 55), medium-differentiated granite (25 < Zr/Hf < 55), and highly differentiated granite (Zr/Hf < 25) [41,42]. Most light-colored granites with a few dark minerals or alaskite have undergone intense crystallization differentiation, also known as strong differentiation or highly differentiated granite. The Zr/Hf ratios of Gaohushan granite range from 17.7 to 32.0, with an average value of 22, suggesting that it may belong to the highly differentiated granite category. On the other hand, the average Zr/Hf ratio for the nearby Ehu granite is 32.85, for Yaoli granite it is 28.47, and for Wolonggu granite it is 27.99 [18,20], indicating that these rocks are medium-differentiated granite. Discrimination diagrams using $10^4 \times Ga/Al$ also show that Gaohushan A-type granites are highly differentiated (Figure 10). The slightly lower Ga/Al ratios (ranging from 1.06×10^4 to 2.71×10^4), as well as the Zr (13.00 to 50.5 ppm) and Y (0.62 to 2.87 ppm) contents of Gaohushan granite, may be attributed to the strong crystallization differentiation of the magma, which caused the fractional crystallization of plagioclase, zircon, and other Y-rich minerals [43].

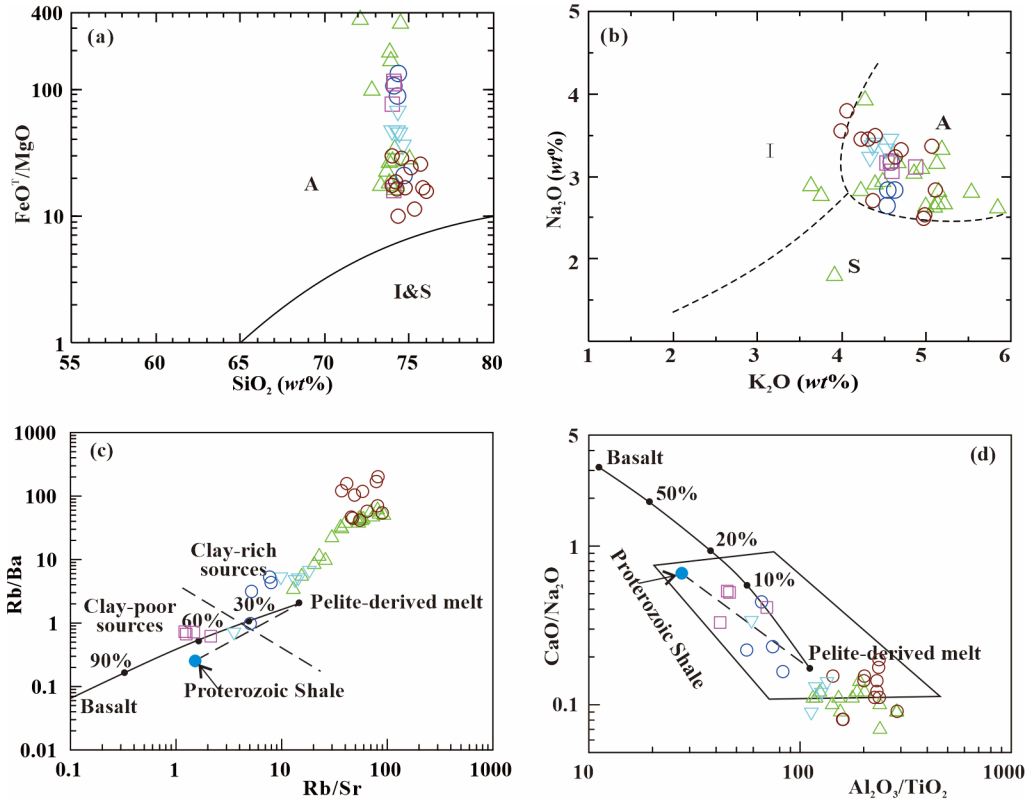

Figure 9. (**a**) FeO^T/MgO vs. SiO_2 discrimination diagram for granites (modified after [44]); (**b**) Na_2O vs. K_2O discrimination diagram for granites (modified after [45]); (**c**) Rb/Sr ratios. (The field of pelite-derived melt and the boundary between clay-poor and clay-rich sources are from [39], and the average compositions of basalt and the average compositions of basalt and Proterozoic shale are from [46]); (**d**) whole-rock CaO/Na_2O vs. Al_2O_3/TiO_2. (data sources and legends shown in Figure 5).

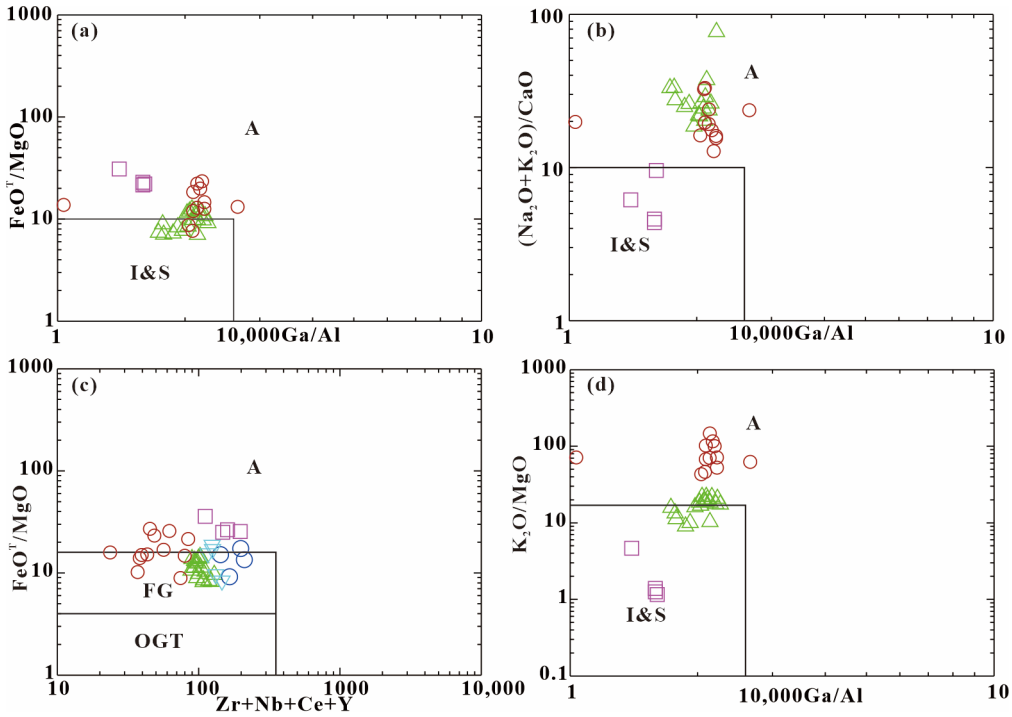

Figure 10. Major elements vs. $10^4 \times$ Ga/Al (**a**,**b**,**d**) and (Zr + Nb + Ce + Y) (**c**) (modified after [35]) (data sources and legends shown in Figure 5).

6.2. Discrimination of A1 or A2 Type for Gaohushan Granite

The R_1 values ($R_1 = 4Si - 11(Na + K) - 2(Fe + Ti)$) of the anorgenic granite range from 500 to 3000. Meanwhile, the R_1 values of post-orogenic type granite are narrow, ranging from 2300 to 2600 [47]. Figure 11 shows that most of the Gaohushan granites are located within the anorgenic granite area in the R_1-R_2 diagram.

Loiselle [48] classified A-type granites as alkaline, metaluminous, and weakly peraluminous rocks, emphasizing their "alkaline, anhydrous, and anorogenic" characteristics. A-type granites are often found intruding into rift zones or stable continental plates, which are referred to as "anorogenic." The Gaohushan A-type granite is high in silicon, highly differentiated, and has a small outcropping area. It belongs to the anorogenic granitoids and formed in the Cretaceous period due to the subduction of the Pacific plate and superdeep faults in the continental crust [49]. The anorogenic and post-orogenic settings of A-type granites are still subject to debate, but it is widely accepted that they form under an extensional tectonic setting [50].

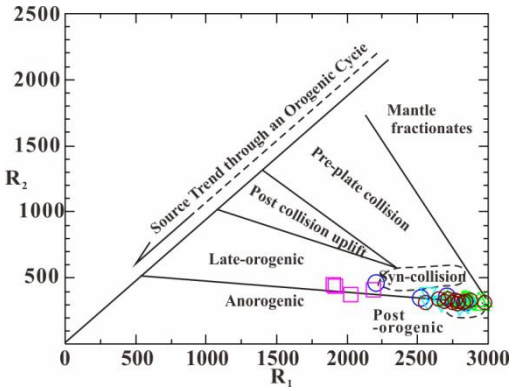

Figure 11. R_1 vs. R_2 diagram for the Gaohushan and adjacent granites (modified after [51]. $R_1 = 4Si - 11 \times (Na + K) - 2 \times (Fe + Ti)$; $R_2 = Al + 2Mg + 6Ca$ (data sources and legends shown in Figure 5).

Eby [38,44] classified A-type granites into A_1-type and A_2-type granite. A_1-type granites are formed in rift environments and are usually associated with hotspots or mantle plumes, while A_2-type granites are mostly formed in post-collisional or post-orogenic settings. The tectonic discrimination diagram in Figure 12 indicates that the Gaohushan A-type granites and adjacent granites in the region fall within the A_1-type granite area, suggesting that these rocks were formed in a rift environment. Additionally, the low contents of rare earth elements (REE) ranging from 2.33 to 23.50 ppm in the Gaohushan granites are consistent with the characteristics of A_1-type granite.

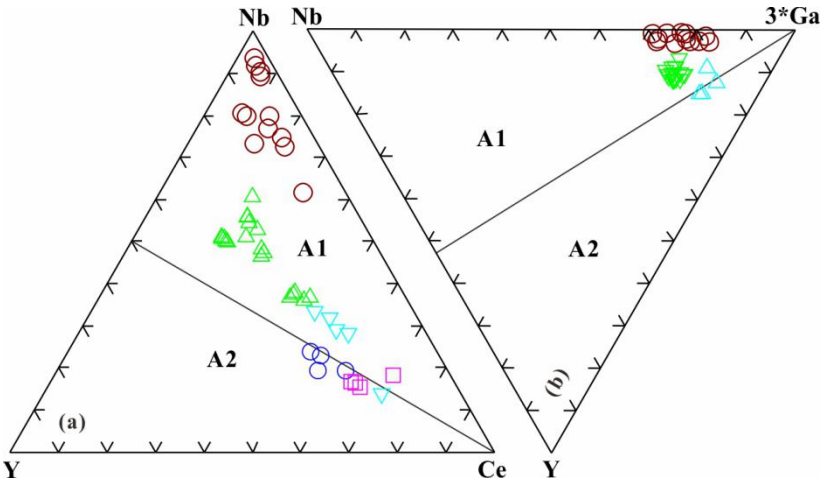

Figure 12. Tectonic discrimination diagrams for A-type granites. (**a**) Nb-Y-Ce diagram. (**b**) Nb-Y-3*Ga diagram. (modified after Eby, [44]) (data sources and legends shown in Figure 5).

6.3. Tectonic Significance

During the Mesozoic era, the paleo-Pacific plate was highly active, leading to the formation of a large active continental margin. While Japan is situated in the volcanic island arc zone, southeastern China is in the back-arc extension zone. As the Pacific plate subducted beneath the South China block, it caused extensive folding and magmatism in the region [52]. In the Early Yanshanian, lithospheric thinning and stretching began in the interior of South China, and this regional lithospheric extension continued periodically until the Cretaceous period [53–56]. The Gaohushan granite was formed at 129.4 ± 1.9 Ma, which coincides with the development of fault basins, intense magmatic activity, and volcanism in South China at 135 ± 5 Ma, as well as the time when inland extension occurred at ~137 Ma [1,57].

During the Early Jurassic period, a 1300 km intracontinental orogenic belt formed in South China, along with a volcanic province in the eastern region, which were linked to low-angle subduction of the Pacific plate and basaltic magma underplating [5,58–60]. This period was characterized by compressional tectonic evolution and geodynamic mechanisms. In the Middle Jurassic, Eastern China experienced a change in tectonic trend from E-W to NE-NNE, and the tectonic setting shifted from a compressional tectonomagmatic orogenic system to an extensional basin and rift system [61,62]. During the Early Cretaceous, a faulted basin and metamorphic core complex emerged, likely due to lithospheric thinning, crust extension-collapse, crust–mantle interaction, and subducting plate melting caused by continental lithospheric delamination and Pacific plate roll-back [63–66]. The tectonic setting shifted into an extensional one in the Early Cretaceous [67,68], during which the A1-type Gaohushan granite was emplaced (Figure 13).

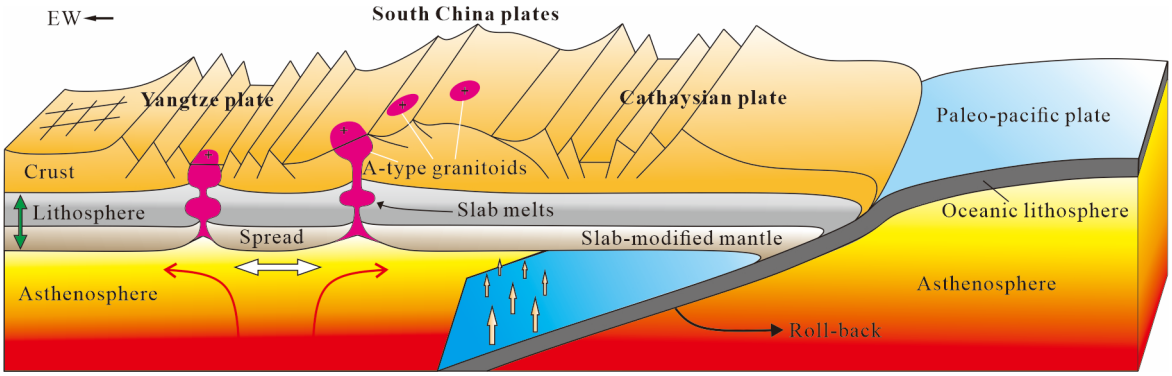

Figure 13. Geodynamic model for the near E–W trending granite belt, which formed in the Early Cretaceous in the northeastern section of the Qin–Hang belt in South China (Modified after [69]).

6.4. Metallogenic Implication

Mao et al. [1] divided the Mesozoic large-scale diagenesis and mineralization in South China into three periods: 170~150 Ma, 140~126 Ma, and 110~80 Ma. These three large-scale diagenesis–mineralization are related to the multi-stage back-arc lithospheric extension, crust–mantle interaction, and deep fluid migration caused by the collision of the South China and North China blocks and the subduction of the oceanic plates [70]. The period from 140 Ma to 126 Ma is a relatively concentrated period of Yanshanian mineralization. The subduction angle of the Pacific slab changed from oblique to almost parallel to the continental margin, which led to the lithospheric extension and thinning [71]. Various deposits from different sources gathered in fault basins and volcanic basins, and mainly have tungsten and tin mineralization [71,72]. The genesis of these deposits is related with granite, and the source of ore-forming materials is related with factors such as the maturity of the crust and the minerality of the strata [73,74]. According to the three mineralization periods divided by Mao et al. [1], the formation age of the Gaohushan granite is 129.4 ± 1.9 Ma, belonging to the second mineralization period under the background of lithospheric extension and thinning, mantle material upwelling, and continental crust remelting.

The highly differentiated granites found in South China are referred to as rare metal or rare element granites, which possess distinctive mineralization properties and are frequently associated with minerals containing tungsten, tin, niobium, tantalum, lithium, beryllium, rubidium, cesium, and rare earth element. The two-mica granite is also often associated with tungsten, tin, and tungsten–tin ore deposits [75,76]. The Gaohushan high-K calc-alkaline A_1-type granites show nearly equivalent contents of K_2O and Na_2O with slightly higher contents of K_2O, and obvious negative Eu anomalies, similar to the characteristics of tungsten–tin mineralized granite (Xihuashan and Piaotang tungsten and tin mining areas). The Gaohushan granites show low ratios of $CaO/(K_2O + Na_2O)$ (from 0.03 to 0.08), low contents of TiO_2, REE and HFSE, and are highly differentiated which is consistent with the geochemical characteristics of Nanling tantalum and niobium granite [77,78]. Therefore, the Gaohushan granite should be an important symbol for the prospecting of W, Sn, Nb, and Ta deposits.

7. Conclusions

(1) The Gaohushan granitic pluton is comprised of two-mica granite, which is a member of the peraluminous high-K calc-alkaline series of rocks. It displays the features of a highly fractionated A-type granite;

(2) The Gaohushan granite crystallized during the Early Cretaceous period, approximately 129.4 ± 1.9 Ma, in an extensional tectonic setting. The magma that formed the granite was derived primarily from the crust, but also had contributions from the mantle;

(3) The A-type granites discovered in the Gaohushan region have similar structural environments and petrochemical characteristics to granites found in tungsten, tin, niobium, and tantalum deposits in southern China. As such, they may serve as important indicators for prospecting these valuable mineral deposits.

Supplementary Materials: The following supporting information can be downloaded at: https://www.mdpi.com/article/10.3390/min13050588/s1, Table S1: LA-ICP-MS zircon rare earth elements analysis of the Gaohushan granite (GHSH); Table S2: LA-ICP-MS zircon Th-U-Pb isotopic analysis of the Gaohushan granite (GHSH); Table S3: major element data components (%) and trace element abundance ($\times 10^{-6}$) of Gaohushan granite.

Author Contributions: This paper was written and the experiments were designed by Z.L. and F.C., and the manuscript was revised by S.L. All authors have read and agreed to the published version of the manuscript.

Funding: This study was funded by the Natural Science Foundation of Guangxi (Grant No. 2020GXNSFAA297091), the National Natural Science Foundation of China (Grant No. 42262026).

Data Availability Statement: Not applicable.

Acknowledgments: We would like to express our sincere gratitude to Jie Yang from Chang'an University for their invaluable assistance during the sample preparation and age analysis processes. We are also grateful for the tremendous help provided by Shanbao Liu of the Institute of Mineral Resources at the Chinese Academy of Geological Sciences, and Anjie Huang of the Northeastern Jiangxi Geological Party, Jiangxi Bureau of Geology and Mineral Exploration, for their logistical support during the sample collection.

Conflicts of Interest: The authors declare no conflict of interest.

References

1. Mao, J.W.; Cheng, Y.B.; Chen, M.H.; Franco, P. Major types and time–space distribution of Mesozoic ore deposits in South China and their geodynamic settings. *Miner. Depos.* **2013**, *48*, 267–294. [CrossRef]
2. Maruyama, S.; Liou, J.G.; Zhang, R. Tectonic evolution of the ultrahigh-pressure (UHP) and high-pressure (HP) metamorphic belts from central China. *Isl. Arc* **1994**, *3*, 112–121. [CrossRef]
3. Gou, X.F.; Qin, Y.; Feng, Z.H.; Li, H.Z.; Huang, Y.G.; Wu, J.; Cui, Y.; Ma, L.F.; Wang, C.Z. U–Pb geochronology and Hf isotope characterization of detrital zircons from Nanhua System of northeastern Guangxi and their constraints on the southwestern suture zone between Yangtze and Cathaysia blocks, South China. *Arab. J. Geosci.* **2022**, *15*, 1769. [CrossRef]
4. Guo, L.Z.; Shi, Y.S.; Lu, H.F.; Ma, R.S.; Dong, H.G.; Yang, S.F. The pre-Devonian tectonic patterns and evolution of South China. *Southeast Asian J. Earth Sci.* **1989**, *3*, 87–93. [CrossRef]
5. Li, S.Z.; Santosh, M.; Zhao, G.C.; Zhang, G.W.; Jin, C. Intracontinental deformation in a frontier of super-convergence: A perspective on the tectonic milieu of the South China Block. *Asian J. Earth Sci.* **2012**, *49*, 313–329. [CrossRef]
6. Mao, J.W.; Zhang, J.D.; Pirajno, F.; Ishiyama, D.; Su, H.M.; Guo, C.L.; Chen, Y.C. Porphyry Cu–Au–Mo–epithermal Ag–Pb–Zn–distal hydrothermal Au deposits in the Dexing area, Jiangxi province, East China—A linked ore system. *Ore Geol. Rev.* **2011**, *43*, 203–216. [CrossRef]
7. Wang, X.L.; Zhou, J.C.; Qiu, J.S.; Zhang, W.L.; Liu, X.M.; Zhang, G.L. LA-ICP-MS U-Pb zircon geochronology of the Neoproterozoic igneous rocks from Northern Guangxi, South China: Implications for tectonic evolution. *Precambr. Res.* **2006**, *145*, 111–130. [CrossRef]
8. Zhang, S.B.; Zheng, Y.F. Formation and evolution of Precambrian continental lithosphere in South China. *Gondwana Res.* **2013**, *23*, 1241–1260. [CrossRef]
9. Deng, J.; Wang, Q.F. Gold mineralization in China: Metallogenic provinces, deposit types and tectonic framework. *Gondwana Res.* **2016**, *36*, 219–274. [CrossRef]
10. Huang, X.D.; Lu, J.J.; Sizaret, S.; Wang, R.H.; Ma, D.S.; Zhang, R.Q.; Zhao, X.; Wu, J.W. Petrogenetic differences between the Middle-Late Jurassic Cu-Pb-Zn-bearing and W-bearing granites in the Nanling Range, South China: A case study of the Tongshanling and Weijia deposits in southern Hunan Province. *China Earth Sci.* **2017**, *60*, 1220–1236. [CrossRef]
11. Li, Z.; Zhou, J.; Mao, J.; Santosh, M.; Yu, M.G.; Li, Y.Q.; Hu, Y.Z.; Langmuir, C.H.; Chen, Z.X.; Cai, X.X.; et al. Zircon U–Pb geochronology and geochemistry of two episodes of granitoids from the northwestern Zhejiang Province, SE China: Implication for magmatic evolution and tectonic transition. *Lithos* **2013**, *179*, 334–352. [CrossRef]
12. Yin, Y.T.; Jin, S.; Wei, W.B.; Lü, Q.T.; Ye, G.F.; Jing, J.e.; Zhang, L.; Dong, H.; Xie, C.L. Lithosphere structure and its implications for the metallogenesis of the Nanling Range, South China: Constraints from 3-D magnetotelluric imaging. *Ore Geol. Rev.* **2021**, *131*, 104064. [CrossRef]

13. Goldfarb, R.J.; Mao, J.W.; Qiu, K.F.; Goryachev, N. The great Yanshanian metallogenic event of eastern Asia: Consequences from one hundred million years of plate margin geodynamics. *Gondwana Res.* **2021**, *100*, 223–250. [CrossRef]
14. Li, S.Z.; Suo, Y.H.; Li, X.Y.; Zhou, J.; Santosh, M.; Wang, P.C.; Wang, G.Z.; Guo, L.L.; Yu, S.Y.; Lan, H.Y.; et al. Mesozoic tectono-magmatic response in the East Asian ocean-continent connection zone to subduction of the Paleo-Pacific Plate. *Earth-Sci. Rev.* **2019**, *192*, 91–137. [CrossRef]
15. Chen, G.H.; Shu, L.S.; Shu, L.M.; Zhang, C.; Ouyang, Y.P. Geological characteristics and mineralization setting of the Zhuxi tungsten (copper) polymetallic deposit in the Eastern Jiangnan Orogen. *China Earth Sci.* **2016**, *59*, 803–823. [CrossRef]
16. Shi, Y.; Xu, Y.X.; Yang, B.; Peng, Z.; Liu, S.Y. Three-dimensional audio-frequency magnetotelluric imaging of Zhuxi copper-tungsten polymetallic deposits, South China. *Geoexploration* **2020**, *172*, 103910. [CrossRef]
17. Han, Y.; Yan, J.; Yang, C.; Wang, S. Zircon age dating and geochronological framwork of the granites in the Taoling-Duanxin area, eastern Jiangnan orogenicbelt. *Mineral. Petrol.* **2019**, *39*, 34–44. (In Chinese with English abstract)
18. Guo, B.R.; Liu, S.W.; Yang, P.T.; Wang, Z.Q.; Luo, P.; Wang, Y.Q.; Luo, G.H.; Wang, W. Petrology, Geochemistry and Pedogenesis of Wolonggu granites and Tongchang granodioritic porphyries: Constraints on copper metallogenic geological settings in northeastern Jiangxi Province. *Geol. Bull. China* **2013**, *32*, 1035–1046. (In Chinese with English abstract)
19. Bai, Y.L.; Wang, Z.Q.; Wang, T.; Wu, F.F. LA-ICP-MS zircon U-Pb age, geochemistry and petrogenesis of the Yaoli pluton in northeastern Jiangxi Province. *Acta Petrol. Mineral.* **2015**, *34*, 35–50. (In Chinese with English abstract)
20. Zhao, P.; Jiang, Y.H.; Liao, S.Y.; Zhou, Q.; Jin, G.D. SHRIMP zircon U-Pb age, Sr-Nd-Hf isotopic geochemistry and petrogenesis of the Ehu pluton in northeastern Jiangxi Province. *Geol. J. China Univ.* **2010**, *16*, 218. (In Chinese with English abstract) [CrossRef]
21. Li, J.H.; Dong, S.W.; Zhang, Y.Q.; Zhao, G.C.; Johnston, S.T.; Cui, J.J.; Xin, Y.J. New insights into Phanerozoic tectonics of south China: Part 1, polyphase deformation in the Jiuling and Lianyunshan domains of the central Jiangnan Orogen. *J. Geophys. Res. Solid Earth* **2016**, *121*, 3048–3080. [CrossRef]
22. Li, L.M.; Lin, S.F.; Xing, G.F.; Davis, D.W.; Jiang, Y.; Davis, W.; Zhang, Y.J. Ca. 830Ma back-arc type volcanic rocks in the eastern part of the Jiangnan orogen: Implications for the Neoproterozoic tectonic evolution of South China Block. *Precambrian Res.* **2016**, *275*, 209–224. [CrossRef]
23. Li, X.H.; Zhao, J.X.; McCulloch, M.T.; Zhou, G.Q.; Xing, F.M. Geochemical and Sm Nd isotopic study of Neoproterozoic ophiolites from southeastern China: Petrogenesis and tectonic implications. *Precambrian Res.* **1997**, *81*, 129–144. [CrossRef]
24. Sun, J.J.; Shu, L.S.; Santosh, M.; Wang, L.S. Precambrian crustal evolution of the central Jiangnan Orogen (South China): Evidence from detrital zircon U-Pb ages and Hf isotopic compositions of Neoproterozoic metasedimentary rocks. *Precambrian Res.* **2018**, *318*, 1–24. [CrossRef]
25. Zhang, Y.Z.; Wang, Y.J. Early Neoproterozoic (∼840Ma) arc magmatism: Geochronological and geochemical constraints on the metabasites in the Central Jiangnan Orogen. *Precambrian Res.* **2016**, *275*, 1–17. [CrossRef]
26. Ludwig, K.R. *Isoplot*, version 3.0; A Geochronological Toolkit for Microsoft Excel. Special publication No. 4, Berkeley Geochronology Center: Berkeley, CA, USA, 2003.
27. Cherniak, D.J.; Watson, E.B. Diffusion in zircon. *Rev. Mineral. Geochem.* **2003**, *53*, 113–143. [CrossRef]
28. Poitrasson, F.; Schaltegger, U.; Hanchar, J.M. Chemistry and physics of accessory minerals: Crystallisation, transformation and geochronological applications. *Chem. Geol.* **2002**, *191*, 1. [CrossRef]
29. Sun, S.S.; McDonough, W.F. Chemical and isotopic systematics of oceanic basalts: Implications for mantle composition and processes. *Misc. Pap.-Geol. Soc.* **1989**, *42*, 313–345. [CrossRef]
30. Middlemost, E.A.K. Naming materials in the magma/igneous rock system. *Earth-Sci. Rev.* **1994**, *37*, 215–224. [CrossRef]
31. Liu, M.Y. Geochemical Genesis of Four Nearly EW Early Cretaceous Granitic Belts in the Eastern Yangtze Block. Bachelor's Thesis, China University of Geosciences, Beijing, China, 2019; pp. 1–68. (In Chinese with English abstract) [CrossRef]
32. Liu, S.B.; Liu, Z.Q.; Wang, C.H.; Wang, D.H.; Zhao, Z.; Hu, Z.H. Geochemical characteristics of REEs and trace elements and Sm-Nd dating of scheelite from the Zhuxi giant tungsten deposit in northeast Jiangxi. *Earth Sci. Front.* **2017**, *24*, 17–30. (In Chinese with English abstract)
33. Streckeisen, A. To each plutonic rock its proper name. *Earth-Sci. Rev.* **1976**, *12*, 1–33. [CrossRef]
34. Rickwood, P.C. Boundary lines within petrologic diagrams which use oxides of major and minor elements. *Lithos* **1989**, *22*, 247–263. [CrossRef]
35. Whalen, J.B.; Currie, K.L.; Chappell, B.W. A-type granites: Geochemical characteristics, discrimination and petrogenesis. *Contrib. Mineral. Petrol.* **1987**, *95*, 407–419. [CrossRef]
36. Wu, F.Y.; Sun, D.Y.; Jahn, B.M.; Wilde, S. A Jurassic garnet-bearing granitic pluton from NE China showing tetrad REE patterns. *Asian J. Earth Sci.* **2004**, *23*, 731–744. [CrossRef]
37. Jahn, B.M.; Wu, F.Y.; Capdevila, R.; Martineau, F.; Zhao, Z.H.; Wang, Y.X. Highly evolved juvenile granites with tetrad REE patterns: The Woduhe and Baerzhe granites from the Great Xing'an Mountains in NE China. *Lithos* **2001**, *59*, 171–198. [CrossRef]
38. Eby, G.N. The A-type granitoids: A review of their occurrence and chemical characteristics and speculations on their petrogenesis. *Lithos* **1990**, *26*, 115–134. [CrossRef]
39. Sylvester, P.J. Post-collisional strongly peraluminous granites. *Lithos* **1998**, *45*, 29–44. [CrossRef]
40. Patiño Douce, A.E.; Johnston, A.D. Phase equilibria and melt productivity in the pelitic system: Implications for the origin of peraluminous granitoids and aluminous granulites. *Contrib. Mineral. Petrol.* **1991**, *107*, 202–218. [CrossRef]

41. Breiter, K.; Škoda, R. Zircon and whole-rock Zr/Hf ratios as markers of the evolution of granitic magmas: Examples from the Teplice caldera (Czech Republic/Germany). *Mineral. Petrol.* **2017**, *111*, 435–457. [CrossRef]
42. Breiter, K.; Lamarão, C.N.; Borges, R.M.K.; Dall'Agnol, R. Chemical characteristics of zircon from A-type granites and comparison to zircon of S-type granites. *Lithos* **2014**, *192–195*, 208–225. [CrossRef]
43. Grebennikov, A.V. A-type granites and related rocks: Petrogenesis and classification. *Russ. Geol. Geophys.* **2014**, *55*, 1353–1366. [CrossRef]
44. Eby, G.N. Chemical subdivision of the A-type granitoids: Petrogenetic and tectonic implications. *Geology* **1992**, *20*, 641–644. [CrossRef]
45. Collins, W.J.; Beams, S.D.; White, A.J.R.; Chappell, B.W. Nature and origin of A-type granites with particular reference to southeastern Australia. *Contrib. Mineral. Petrol.* **1982**, *80*, 189–200. [CrossRef]
46. Conway, C.M.; Condie, K.C.; Noll, P.D. Geochemical and detrital mode evidence for two sources of Early Proterozoic sedimentary rocks from the Tonto Basin Supergroup, central Arizona—Reply. *Sediment. Geol.* **1993**, *87*, 241–244. [CrossRef]
47. Hong, D.W.; Wang, S.G.; Han, B.F.; Jin, M.Y. Post-orogenic alkaline granites from China and comparisons with anorogenic alkaline granites elsewhere. *Southeast Asian J. Earth Sci.* **1996**, *13*, 13–27. [CrossRef]
48. Loiselle, M.C. Characteristics and origin of anorogenic granites. *Geol. Soc. Am.* **1979**, *41*, 468. [CrossRef]
49. Chopin, C. Ultrahigh-pressure metamorphism: Tracing continental crust into the mantle. *Earth Planet. Sci. Lett.* **2003**, *212*, 1–14. [CrossRef]
50. Bonin, B. A-type granites and related rocks: Evolution of a concept, problems and prospects. *Lithos* **2007**, *97*, 1–29. [CrossRef]
51. Batchelor, R.A.; Bowden, P. Petrogenetic interpretation of granitoid rock series using multicationic parameters. *Chem. Geol.* **1985**, *48*, 43–55. [CrossRef]
52. Shu, L.S.; Yao, J.L.; Wang, B.; Faure, M.; Charvet, J.; Chen, Y. Neoproterozoic plate tectonic process and Phanerozoic geodynamic evolution of the South China Block. *Earth-Sci. Rev.* **2021**, *216*, 103596. [CrossRef]
53. Kusky, T.M.; Windley, B.F.; Zhai, M.G. Tectonic evolution of the North China Block: From orogen to craton to orogen. *Misc. Pap.-Geol. Soc.* **2007**, *280*, 1–34. [CrossRef]
54. Li, X.H.; Li, Z.X.; Ge, W.C.; Zhou, H.W.; Li, W.X.; Liu, Y.; Wingate, M.T.D. Neoproterozoic granitoids in South China: Crustal melting above a mantle plume at ca. 825 Ma? *Precambrian Res.* **2003**, *122*, 45–83. [CrossRef]
55. Mai, H.A.; Chan, Y.L.; Yeh, M.W.; Lee, T.Y. Tectonic implications of Mesozoic magmatism to initiation of Cenozoic basin development within the passive South China Sea margin. *Int. J. Earth Sci.* **2018**, *107*, 1153–1174. [CrossRef]
56. Zhou, J.; Li, S.Z.; Suo, Y.H.; Zhang, L.; Du, X.D.; Cao, X.Z.; Wang, G.Z.; Li, F.K.; Liu, Z.; Liu, J.; et al. NE-trending transtensional faulting in the Pearl River Mouth basin of the Northern South China Sea margin. *Gondwana Res.* **2022**. [CrossRef]
57. Wang, Z.J.; Wang, J.; Duan, T.Z.; Xie, Y.; Zhuo, J.W.; Yang, P. Geochronology of middle Neoproterozoic volcanic deposits in Yangtze Craton interior of South China and its implications to tectonic settings. *China Earth Sci.* **2010**, *53*, 1307–1315. [CrossRef]
58. Cawood, P.A.; Kröner, A.; Collins, W.J.; Kusky, T.M.; Mooney, W.D.; Windley, B.F. Accretionary orogens through Earth history. *Misc. Pap.-Geol. Soc.* **2009**, *318*, 1–36. [CrossRef]
59. Pirajno, F.; Ernst, R.E.; Borisenko, A.S.; Fedoseev, G.; Naumov, E.A. Intraplate magmatism in Central Asia and China and associated metallogeny. *Ore Geol. Rev.* **2009**, *35*, 114–136. [CrossRef]
60. Windley, B.F.; Maruyama, S.; Xiao, W.J. Delamination/thinning of sub-continental lithospheric mantle under Eastern China: The role of water and multiple subduction. *Am. J. Sci.* **2010**, *310*, 1250–1293. [CrossRef]
61. Ju, Y.W.; Yu, K.; Wang, G.Z.; Li, W.Y.; Zhang, K.J.; Li, S.H.; Guo, L.L.; Sun, Y.; Feng, H.Y.; Qiao, P.; et al. Coupling response of the Meso–Cenozoic differential evolution of the North China Craton to lithospheric structural transformation. *Earth-Sci. Rev.* **2021**, *223*, 103859. [CrossRef]
62. Ma, H.M.; Wang, Y.; Huang, Y.J.; Xie, Y.T. Three-stage Mesozoic intracontinental tectonic evolution of South China recorded in an overprinted basin: Evidence from stratigraphy and detrital zircon U–Pb dating. *Geol. Mag.* **2019**, *156*, 2085–2103. [CrossRef]
63. Goss, S.C.; Wilde, S.A.; Wu, F.Y.; Yang, J.H. The age, isotopic signature and significance of the youngest Mesozoic granitoids in the Jiaodong Terrane, Shandong Province, North China Craton. *Lithos* **2010**, *120*, 309–326. [CrossRef]
64. Hamilton, W.B. Subduction systems and magmatism. *Misc. Pap.-Geol. Soc.* **1994**, *81*, 3–28. [CrossRef]
65. Li, X.H.; Fan, H.R.; Hu, F.F.; Hollings, P.; Yang, K.F.; Liu, X. Linking lithospheric thinning and magmatic evolution of late Jurassic to early cretaceous granitoids in the Jiaobei Terrane, southeastern North China Craton. *Lithos* **2019**, *324–325*, 280–296. [CrossRef]
66. Liu, J.G.; Cai, R.H.; Pearson, D.G.; Scott, J.M. Thinning and destruction of the lithospheric mantle root beneath the North China Craton: A review. *Earth-Sci. Rev.* **2019**, *196*, 102873. [CrossRef]
67. Gaina, C.; Roest, W.R.; Müller, R.D. Late Cretaceous–Cenozoic deformation of northeast Asia. *Earth Planet. Sci. Lett.* **2002**, *197*, 273–286. [CrossRef]
68. Kamp, P.J.J. Late Cretaceous-Cenozoic tectonic development of the southwest pacific region. *Tectonophysics* **1986**, *121*, 225–251. [CrossRef]
69. Yang, Y.Z.; Wang, Y.; Ye, R.S.; Li, S.Q.; He, J.F.; Siebel, W.; Chen, F.K. Petrology and geochemistry of Early Cretaceous A-type granitoids and late Mesozoic mafic dikes and their relationship to adakitic intrusions in the lower Yangtze River belt, Southeast China. *Int. Geol. Rev.* **2017**, *59*, 62–79. [CrossRef]
70. Zhu, R.X.; Zheng, T.Y. Destruction geodynamics of the North China craton and its Paleoproterozoic plate tectonics. *Chin. Sci. Bull.* **2009**, *54*, 3354–3366. [CrossRef]

71. Li, Q.; Zhao, K.D.; Lai, P.C.; Jiang, S.Y.; Chen, W. Petrogenesis of Cretaceous volcanic-intrusive complex from the giant Yanbei tin deposit, South China: Implication for multiple magma sources, tin mineralization, and geodynamic setting. *Lithos* **2018**, *296–299*, 163–180. [CrossRef]
72. Liu, Y.; Cheng, Q.M.; Xia, Q.L.; Wang, X.Q. Mineral potential mapping for tungsten polymetallic deposits in the Nanling metallogenic belt, South China. *J. Earth Sci.* **2014**, *25*, 689–700. [CrossRef]
73. Baker, T.; Pollard, P.J.; Mustard, R.; Mark, G.; Graham, J.L. A comparison of granite-related tin, tungsten, and gold-bismuth deposits: Implications for exploration. *SEG Discov.* **2005**, *61*, 5–17. [CrossRef]
74. Plimer, I.R. Fundamental parameters for the formation of granite-related tin deposits. *Geol. Rundsch.* **1987**, *76*, 23–40. [CrossRef]
75. Oosterom, M.G.; Bussink, R.W.; Vriend, S.P. Lithogeochemical studies of aureoles around the Panasqueira tin-tungsten deposit, Portugal. *Miner. Depos.* **1984**, *19*, 283–288. [CrossRef]
76. Zhang, R.Q.; Lu, J.J.; Lehmann, B.; Li, C.Y.; Li, G.L.; Zhang, L.P.; Guo, J.; Sun, W.D. Combined zircon and cassiterite U–Pb dating of the Piaotang granite-related tungsten–tin deposit, southern Jiangxi tungsten district, China. *Ore Geol. Rev.* **2017**, *82*, 268–284. [CrossRef]
77. Luo, Z.Y.; Li, H.; Wu, J.H.; Sun, W.B.; Zhou, J.Q.; Maulana, A. Geochronology and geochemistry of the Xianghualing granitic rocks: Insights into multi-stage Sn-polymetallic mineralization in South China. *Minerals* **2022**, *12*, 1091. [CrossRef]
78. Zhao, Z.; Yang, X.Y.; Liu, Q.Y.; Lu, Y.Y.; Chen, S.S.; Sun, C.; Zhang, Z.Z.; Wang, H.; Li, S. In-situ boron isotopic and geochemical compositions of tourmaline from the Shangbao Nb–Ta bearing monzogranite, Nanling Range: Implication for magmatic-hydrothermal evolution of Nb and Ta. *Lithos* **2021**, *386–387*, 106010. [CrossRef]